

Dynamical properties of two coupled quantum cavities with single-mode amplification

Original

Dynamical properties of two coupled quantum cavities with single-mode amplification / Penna, V., Raffa, F.. - In: PHYSICAL REVIEW. E. - ISSN 2470-0045. - 110:(2024), pp. 1-11. [10.1103/PhysRevE.110.044126]

Availability:

This version is available at: 11583/2993593 since: 2024-11-15T12:26:12Z

Publisher:

American Physical Society

Published

DOI:10.1103/PhysRevE.110.044126



Terms of use:

This article is made available under terms and conditions as specified in the corresponding bibliographic description in the repository

Publisher copyright

(Article begins on next page)

Dynamical properties of two coupled quantum cavities with single-mode amplification

V. Penna  and F. A. Raffa 

Dipartimento di Scienza Applicata e Tecnologia, Politecnico di Torino, Corso Duca degli Abruzzi 24, I-10129 Torino, Italy



(Received 15 May 2024; accepted 19 September 2024; published 18 October 2024)

Coupled optical cavities provide one of the simplest possible schemes to engineer the interaction of bosonic modes. This paper investigates a two-mode model where, in addition to the usual mode coupling, the presence of an amplification term associated to one of the modes triggers an unexpectedly rich dynamical scenario. The resulting nontrivial model is diagonalized by implementing the dynamical-algebra method, a group-theoretic approach which allows one to determine the stability diagram of the model Hamiltonian in terms of the two mode frequencies for given values of the interaction and amplification parameters. The mode interaction significantly modifies the simple amplification effect of the noninteracting model causing the separation of the unstable domain (where the amplification takes place) into two subdomains, one of which is stable, features no amplification effect, and exhibits an extension controlled by the interaction parameter. The analysis of stability properties is corroborated by the fully analytic study of the energy spectrum which exhibits the transition from a discrete to a continuous structure whenever the system undergoes the transition from a stable region to an unstable region where the amplification effect occurs. This scenario is further confirmed by the calculation of the time evolution of the mode populations.

DOI: [10.1103/PhysRevE.110.044126](https://doi.org/10.1103/PhysRevE.110.044126)

I. INTRODUCTION

The study of coupled optical cavities has received increasing attention in the last two decades due to a rich phenomenology which involves different fields of physics and gives one the opportunity to explore a variety of critical phenomena within a fully quantum environment. Manifold realizations of coupled optical cavities have been designed and realized at the experimental level. For example, in photon Josephson junctions [1,2], cavities consist of microwave resonators which, in addition to the exchange of photons caused by the intercavity tunneling, feature the coupling with superconducting qubits. On the other hand, laser-driven cavities containing a nonlinear crystal feature the coupling of the fundamental and second-harmonic modes of each cavity [3], while two-photon cavities (see [4–6], among many others), represented within the Bose-Hubbard (BH) picture [7], describe the interplay between the effect of Kerr nonlinearity and intercavity tunneling. Furthermore, it is worth mentioning optomechanical devices where, in addition to the coupling of the optical modes of two resonators, the control of phonon lasing takes into account the effect of the interaction with a mechanical mode supported by one of the resonators [8,9].

With respect to the previous mode-coupling schemes, the present paper investigates a minimal model of two interacting bosonic modes focusing on the nontrivial role played by the quadratic amplification of one of such modes. The relevant Hamiltonian, in units $\hbar = 1$, reads

$$H = wa^\dagger a + vb^\dagger b + g(a^\dagger b + ab^\dagger) + \sigma(a^2 + a^{\dagger 2}), \quad (1)$$

where a (a^\dagger) and b (b^\dagger) are the annihilation (creation) operators relevant to frequencies w and v , obeying the commutation relations $[a, a^\dagger] = 1$, $[b, b^\dagger] = 1$. Parameter g describes the interaction between the modes a and b associated to two optical cavities, while σ adds the quadratic-amplification effect of

one of the two modes. The mode frequencies w and v , together with g and σ , span the four-dimensional parameter space of the system.

Interestingly, other classes of systems can be mentioned which, when introducing an amplification term, essentially reduce to model (1). For example, within quantum optics, a representative system is the Tavis-Cummings (TC) model [10,11] of N two-level atoms sharing the same level splitting v and interacting with the single bosonic mode a through an atom-radiation coupling of intensity g . The corresponding Hamiltonian

$$H_{\text{TC}} = wa^\dagger a + vJ_z + \frac{g}{\sqrt{N}}(aJ_+ + a^\dagger J_-)$$

exhibits collective operators J_z , J_- , and J_+ that result from the addition of the spin operators of each two-level atom and satisfy the commutators $[J_z, J_\pm] = \pm J_\pm$, $[J_+, J_-] = 2J_z$ of the algebra $\text{su}(2)$. This model, apart from the amplification term, easily reduces to a Hamiltonian contained in model (1) thanks to the Holstein-Primakoff realization [12] of $\text{su}(2)$. The latter allows one to represent the collective operators with a new bosonic mode b such that, in the thermodynamic limit of $N \rightarrow \infty$, $J_+ \simeq b^\dagger \sqrt{N}$, $J_- = J_+^\dagger$, and $J_z = b^\dagger b - N/2$. This interpretation in quantum-optical terms can be extended to the more general Dicke model, whose realizations are extensively utilized in the analysis of cavity quantum electrodynamics systems and of quantum phase transitions [13–18]. Further examples are provided by the model Hamiltonian describing a binary boson mixture trapped in two potential wells which in the superfluid regime exhibits interaction-dependent amplification terms [19], and the ring-ladder Hamiltonian describing the coupling of two BH circuits [20] which feature amplification terms when implementing the Bogoliubov-approximation approach. Lastly, it is worth mentioning the anisotropic Hopfield model, closely related

to Hamiltonian (1), whose analytical solution is derived in Ref. [21] leading to a thorough analysis of the spectral and thermometric properties of this model.

This paper investigates the dynamical properties of model (1) as determined by the interplay of the four parameters w , v , g , and σ . One should recall that, for $g = 0$, model (1) reduces to the well-known Hamiltonian describing the degenerate-parametric down conversion (PDC) [22] whose mode population, in addition to a stable oscillatory regime, is characterized by an unstable regime, controlled by σ , triggering the amplification effect (see, e.g., [23]). Note that mode b is, in this case, an independent feature. On the other hand, for $\sigma = 0$, model (1) reduces to two coupled bosonic modes whose realization is discussed, for example, in Refs. [2,3] (coupled cavities) and [24,25] (atomtronic devices). The combined action of the amplification effect in one of the two modes with the coupling with a second mode leads to a more structured model whose diagonalization is far from trivial and suggests the possibility to observe a richer phenomenology.

To this end, after showing that model (1) belongs to the symplectic Lie algebra $\mathfrak{sp}(4)$, the dynamical-algebra method is applied which allows one to take the relevant Hamiltonian into a diagonal form and to recognize the stable and unstable regimes that the model features. This, in turn, leads to the construction of the stability diagram \mathcal{D} , namely, the domain of stable and unstable regions in the parameter space described by w and v at given g and σ . The study of spectral properties of the model and the derivation of the time evolution of the average boson population of each mode provide an effective characterization of stable and unstable regimes which validate the structure of \mathcal{D} . Interestingly, the stability diagram, which for $g = 0$ exhibits a stable region and an unstable amplification region controlled by σ , for $g \neq 0$, is shown to feature an unexpected splitting of the amplification region into two subregions, one of which exhibits a stable character and no amplification effect.

The outline of the work is as follows. In Sec. II, using the dynamical-algebra method, Hamiltonian (1) is taken into a diagonal form, and the stability and instability domains are identified. With $k = w - 2\sigma$, such analysis is carried out for various ranges of the system parameters. The analytical calculations include both the case $k > 0$, with the further distinction between weak ($g^2 < kv$) and strong ($g^2 > kv$) coupling, and the case $k < 0$. Section III is devoted to highlight the changes of the energy spectrum of Hamiltonian (1) as the system crosses the boundaries between stable and unstable domains. In Sec. IV, the dynamics of the system is analyzed in terms of the expectation values of the number operators $a^\dagger a$ and $b^\dagger b$ which make visible the effect of the amplification. The structure of the stability diagram is discussed in Sec. V. Final remarks are contained in Sec. VI. Appendices A–D contain supplemental material concerning the mathematical calculations of the diagonalization process and the time evolution of the two modes.

II. SOLUTION OF THE TWO-CAVITY MODEL

The solution of the model, namely, the identification of the spectrum of Hamiltonian H and of the relevant energy eigenstates, can be found by implementing the dynamical-algebra

method [26–28]. Such procedure can be applied whenever the Hamiltonian belongs to a Lie algebra \mathcal{A} (the dynamical algebra) and thus can be represented as a linear combination $H = \sum_k h_k E_k$, $h_k \in \mathbb{R}$ of the algebra generators E_k . The latter satisfy commutators $[E_k, E_n] = f_{knm} E_m$ which univocally define the properties of \mathcal{A} through the structure constants f_{knm} . Within the Lie-group theory [29], the knowledge of \mathcal{A} allows one to construct the group G of unitary transformations U whose distinctive property is that, if $H \in \mathcal{A}$, then the action of U , $UHU^\dagger = H' \in \mathcal{A}$, always generates an element of the algebra. The crucial point in the solution process consists in determining the transformation U for which H' takes a diagonal form, and in defining a suitable disentangled form $U = U_1 U_2 \dots U_N$ whose factors $U_i \in G$ are the elementary transformations which optimize the derivation of H' [30,31]. To apply this method it is convenient rewriting H in terms of momenta p and P and position variables x and X implicitly defined by

$$a = \frac{x + ip}{\sqrt{2}}, \quad b = \frac{X + iP}{\sqrt{2}}, \quad (2)$$

with commutators $[x, p] = [X, P] = 1$. Up to a constant term, the Hamiltonian takes the form

$$H = \frac{1}{2}(ux^2 + kp^2) + \frac{v}{2}(P^2 + X^2) + g(xX + pP), \quad (3)$$

where $k = w - 2\sigma$, $u = w + 2\sigma$. The quantities $x^2 \pm p^2$, $P^2 + X^2$, $xX + pP$ are recognized to be four of the ten generators of the algebra $\mathcal{A} = \mathfrak{sp}(4)$. Then the diagonalization process involves the transformations of the symplectic group $G = \text{Sp}(4)$. This group, the relevant algebra, and its commutators are reviewed in [30]. A similar approach, based on algebra $\mathfrak{su}(2)$, was used in [32] to diagonalize a non-Hermitian effective decay model.

A. Regime $k > 0, g^2 < kv$

The inequality $g^2 < kv$, which emerges in the diagonalization process, can be seen as the condition implicitly defining the weak-interaction regime since g^2 is smaller than the product of the mode frequencies $kv \simeq wv$ if σ is small enough. This implies as well $k > 0$, a condition that, unless otherwise stated, is assumed throughout the subsequent discussion. The form (3) of H suggests that the transformation which diagonalizes H features a three-step process and thus can be written as $U = R_\mu D_\alpha R_\phi$ where

$$R_\phi = e^{i\phi(xP - Xp)}, \quad D_\alpha = e^{i\alpha(xp - XP)}$$

represent a standard rotation and a squeezing transformation, respectively, generated by the algebra elements $xP - Xp$ and $xp - XP$. A second rotation R_μ is included which is parametrized by a different angle μ . Their action is defined by

$$R_\phi x R_\phi^\dagger = c_\phi x + s_\phi X, \quad R_\phi p R_\phi^\dagger = c_\phi p + s_\phi P, \quad (4)$$

$$R_\phi X R_\phi^\dagger = c_\phi X - s_\phi x, \quad R_\phi P R_\phi^\dagger = c_\phi P - s_\phi p, \quad (5)$$

$$D_\alpha x D_\alpha^\dagger = x e^\alpha, \quad D_\alpha p D_\alpha^\dagger = p e^{-\alpha}, \quad (6)$$

$$D_\alpha X D_\alpha^\dagger = X e^{-\alpha}, \quad D_\alpha P D_\alpha^\dagger = P e^\alpha, \quad (7)$$

where the shorthand notation $c_\phi = \cos \phi$, $s_\phi = \sin \phi$ has been used. The first step leads to the Hamiltonian

$$H_1 = R_\phi H R_\phi^\dagger = (k + v + \rho) \frac{p^2}{4} + (k + v - \rho) \frac{P^2}{4} + V(x, X),$$

$$V(x, X) = \left(\frac{u + v}{4} + \xi \right) x^2 + \left(\frac{u + v}{4} - \xi \right) X^2 + \frac{(k - u)g}{\rho} xX$$

with

$$\rho = \sqrt{(k - v)^2 + 4g^2}, \quad \xi = \frac{(u - v)(k - v) + 4g^2}{4\rho}.$$

This transformation shows how the term pP can be removed from H by imposing the condition

$$\tan 2\phi = -\frac{2g}{k - v}.$$

In H_1 the kinetic energy term is positive since $k + v - \rho > 0$ is ensured by $g^2 < kv$. This circumstance suggests that if we succeed in reducing the kinetic energy to $p^2 + P^2$, then, by exploiting its invariance under the rotation action, a final rotation R_μ is sufficient to remove the interaction term xX in the potential of H_1 thereby generating a diagonal Hamiltonian. To achieve this goal, the second step thus consists in utilizing transformation D_α which gives

$$H_2 = D_\alpha H_1 D_\alpha^\dagger = \frac{\gamma}{4}(p^2 + P^2) + \frac{\mu}{4}(x^2 + X^2) + \frac{A(x^2 - X^2) + DxX}{4\rho\gamma}, \quad (8)$$

where

$$\gamma = \sqrt{(k + v)^2 - \rho^2} \equiv 2\sqrt{kv - g^2}, \quad D = 4\gamma g(k - u),$$

$$A = (u + v)\rho^2 + (k + v)(\rho^2 + (u - k)(k - v)),$$

and

$$\mu = \frac{(u + v)(k + v) + \rho^2 + (u - k)(k - v)}{\gamma}.$$

The condition on parameter α in D_α

$$e^{2\alpha} = \sqrt{\frac{k + v + \rho}{k + v - \rho}} \quad (9)$$

must be imposed to obtain p^2 and P^2 with the same coefficient. This leads to the third final step where rotation R_μ enables us to obtain a diagonal Hamiltonian describing two independent harmonic oscillators

$$H_3 = R_\mu H_2 R_\mu^\dagger = \frac{\gamma}{4}(p^2 + P^2) + \frac{\sigma_+}{4\gamma} x^2 + \frac{\sigma_-}{4\gamma} X^2, \quad (10)$$

where

$$\sigma_\pm = \Delta \pm \frac{\sqrt{D^2 + 4A^2}}{2\rho}, \quad (11)$$

and $\Delta = \rho^2 + (u - k)(k - v) + (k + v)(u + v)$. Note that $\gamma > 0$ is always valid, while $\Delta > 0$ can be shown to be satisfied if $\sqrt{2}\sigma < g$ meaning that the amplification parameter

must be sufficiently small. Additionally, the unknown parameter μ defined through the condition

$$\tan 2\mu = -\frac{D}{2A}$$

allows one to remove the coupling term xX from $R_\mu H_2 R_\mu^\dagger$. While the xp oscillator is always stable because $\gamma > 0$ and the coefficient of x^2 can be shown to be always positive, the XP oscillator is stable only in a restricted region \mathcal{D}_1 of the w - v plane, identified by

$$\Delta - \frac{\sqrt{D^2 + 4A^2}}{2\rho} > 0 \Leftrightarrow v > F_-(w) = \frac{g^2}{w - 2\sigma}, \quad (12)$$

together with $k \geq 0$. One should recall that the latter inequality is equivalent to the condition $kv > g^2$. Its violation leads one to explore the instability regime of H .

B. Regime $k > 0$, $g^2 > kv$

The new condition $g^2 > kv$, defining the strong interaction regime, significantly modifies the structure of Hamiltonian H_1 found in Sec. II A. In particular, the coefficient of term P^2 becomes negative since $g^2 > kv$ entails $k + v - \rho < 0$. The reduction of the Hamiltonian H_1 (and thus of H) to a diagonal form then begins with

$$H_1 = R_\phi H R_\phi^\dagger = (k + v + \rho) \frac{p^2}{4} - (\rho - k - v) \frac{P^2}{4} + V(x, X),$$

where the presence of the negative coefficient of P^2 affects the entire diagonalization process. Unlike the case $g^2 < kv$, this involves the new transformation $U = S_\theta D_\alpha R_\phi$ which, in addition to a rotation and a squeezing transformation, now includes the hyperbolic transformation $S_\theta = e^{i\theta(xP + Xp)}$. Its action is defined by

$$S_\theta x S_\theta^\dagger = c_\theta x + s_\theta X, \quad S_\theta p S_\theta^\dagger = c_\theta p - s_\theta P, \\ S_\theta X S_\theta^\dagger = c_\theta X + s_\theta x, \quad S_\theta P S_\theta^\dagger = c_\theta P - s_\theta p,$$

with $c_\theta = \cosh \theta$ and $s_\theta = \sinh \theta$. The inclusion in U of this transformation is due to the fact that $p^2 - P^2$ is invariant under the action of S_θ . In light of this, it is advantageous to reduce H_1 to a form in which p^2 and P^2 exhibit the same coefficient. To this end, we assume that the parameter α in D_α is defined by

$$e^{2\alpha} = \sqrt{\frac{k + v + \rho}{\rho - k - v}}, \quad (13)$$

where $\rho - k - v > 0$ is ensured by $kv < g^2$. The subsequent action of S_θ [see Eq. (B3)] leads to the final (diagonal) Hamiltonian

$$H_3 = U H U^\dagger = \frac{\eta}{4} p^2 + \frac{\tau_+}{4\eta} x^2 - \frac{\eta}{4} P^2 - \frac{\tau_-}{4\eta} X^2, \quad (14)$$

where $\eta = \sqrt{\rho^2 - (k + v)^2} = 2\sqrt{g^2 - kv}$ and

$$\tau_\pm = \chi \pm \sqrt{B}, \quad \chi = uk + v^2 + 2g^2,$$

with

$$B = 4g^2(k + v)(u + v) + (uk - v^2)^2.$$

This Hamiltonian features a stable character if, in addition to $g^2 > kv$, the inequality $\sqrt{B} < \chi$ is satisfied. Such conditions

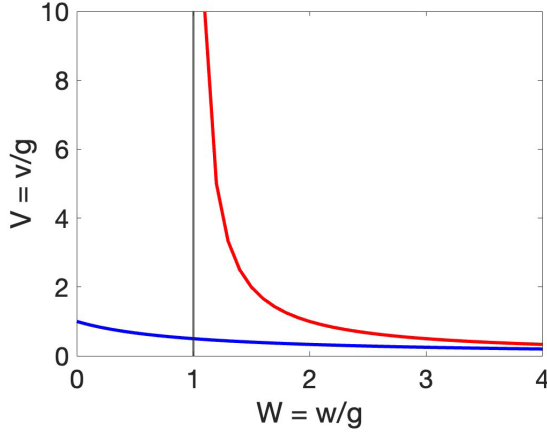


FIG. 1. Representation of curves (17), written in terms of dimensionless variables $V = v/g$, $W = w/g$, $\Sigma = \sigma/g$ for $\sigma = 0.5$ and $g = 1.0$. The resulting curves are $V = F_{\pm}(W) = 1/(W \pm 2\Sigma)$. The red (upper) curve $V = F_-(W)$ and the blue (lower) curve $V = F_+(W)$ separate stable domains \mathcal{D}_1 and \mathcal{D}_2 , respectively, from the intermediate unstable domain \mathcal{D}_3 .

are expressed by

$$v < f_-(w) = \frac{g^2}{w - 2\sigma}, \quad v < f_+(w) = \frac{g^2}{w + 2\sigma}, \quad (15)$$

respectively. Note that, in the infinite portion $w \geq 2\sigma$ of the w - v plane representing the *stability diagram* \mathcal{D} , the second inequality implicitly validates the first one and defines a second stability domain \mathcal{D}_2 . In this case, \mathcal{H}_3 is the linear combination of two harmonic-oscillator Hamiltonians exhibiting the customary discrete spectrum and a well-defined set of eigenstates.

On the other hand, the region intercalating the two stability domains in \mathcal{D} , where $v < f_-(w)$ and $v > f_+(w)$, implicitly identifies an instability domain \mathcal{D}_3 . In this case, Hamiltonian

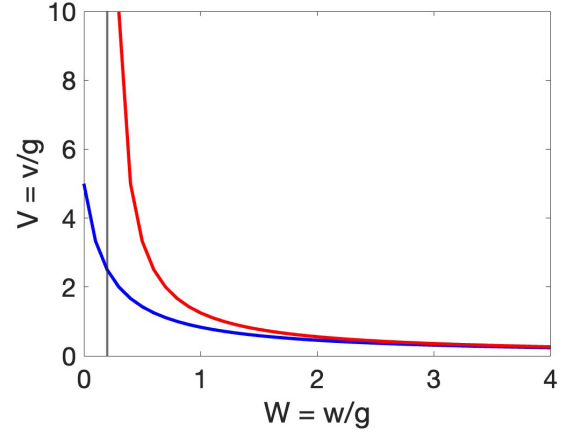


FIG. 3. Dimensionless representation of boundaries (17) for $\sigma = 0.1$ and $g = 1.0$ with $W = w/g$, $\Sigma = \sigma/g$, and $V = v/g$ related to curves $V = F_{\pm}(W)$ as in Fig. 1. The comparison with Fig. 1 shows how decreasing Σ entails that the extension of \mathcal{D}_3 reduces accordingly. For $\Sigma \rightarrow 0$ the asymptote tends to the vertical axis while the blue lower curve tends to the red upper one, namely, $V = F_+(W) \rightarrow V = F_-(W) = 1/W$. \mathcal{D}_1 and \mathcal{D}_2 merge in a unique domain while the instability domain \mathcal{D}_3 vanishes.

(14) becomes

$$\mathcal{H}_3 = \frac{\eta}{4}p^2 + \frac{\tau_+}{4\eta}x^2 - \left(\frac{\eta}{4}P^2 - \frac{\tau_-}{4\eta}X^2 \right), \quad (16)$$

where $\tau_{\pm} = |\sqrt{B} \pm \chi|$, and the condition $\sqrt{B} - \chi > 0$ implies that, in addition to an xp harmonic oscillator, \mathcal{H}_3 features a XP inverted oscillator [33–36]. Interestingly, while the xp oscillator corresponds to an element of the compact subalgebra $\mathfrak{su}(2)$ of the dynamical algebra \mathcal{A} , the inverted oscillator essentially represents a noncompact generator of the subalgebra $\mathfrak{su}(1,1)$ of \mathcal{A} . These features can be shown to determine completely different dynamical behaviors in the two cases.

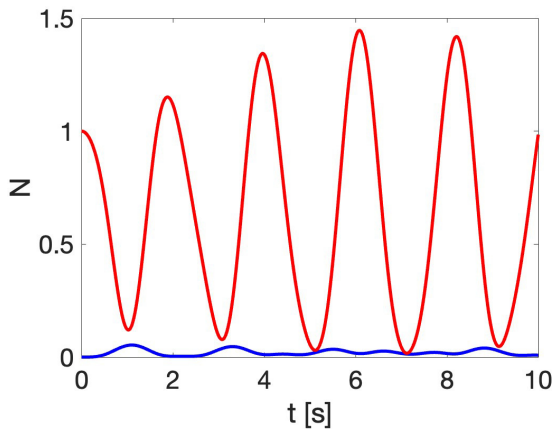


FIG. 2. Time evolution of the mode- a population N described by Eq. (26). The model parameters, referred to in Fig. 1, are $w = 2.0$, and $v = 4.0$ with $\sigma = 0.5$, and $g = 1.0$. This choice corresponds to a point in the stable domain \mathcal{D}_1 . For $\alpha = \beta = 1$, the population exhibits (red upper line) oscillations depending on two frequencies [see Eq. (25)]. The blue lower line corresponds to the vacuum-state oscillations.

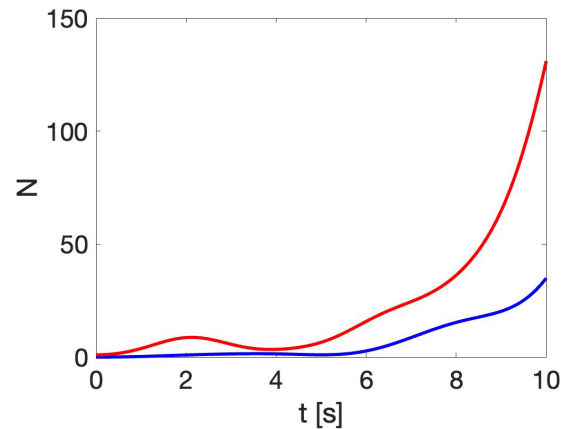


FIG. 4. Time evolution of the mode- a population N described by Eq. (30). The model parameters, referred to in Fig. 1, are $w = 1.5$, and $v = 1.0$ with $\sigma = 0.5$, and $g = 1.0$. This choice corresponds to a point in the unstable domain \mathcal{D}_2 . For $\alpha = \beta = 1$, the population exhibits (red upper line) a diverging behavior controlled by parameter $\sqrt{\tau_-}$ [see Eq. (29)]. The blue lower line corresponds to the vacuum-state evolution.

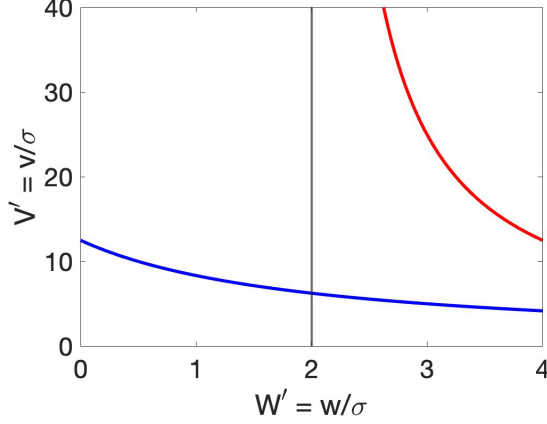


FIG. 5. Curves $V' = G_{\pm}(W') = \Gamma^2/(W' \pm 2)$, representing boundaries (17), for $\sigma = 1.0$ and $g = 5.0$, in terms of dimensionless variables $V' = v/\sigma$, $W' = w/\sigma$, and $\Gamma = g/\sigma$. The red (upper) curve and the blue (lower) curve separate stable and unstable domains.

Figures 1, 3, 5, and 6 illustrate the two curves

$$v = f_-(w) = \frac{g^2}{w - 2\sigma}, \quad v = f_+(w) = \frac{g^2}{w + 2\sigma}, \quad (17)$$

bounding for $w > 2\sigma$ the stability domains \mathcal{D}_1 and \mathcal{D}_2 from below (red curve) and from above (blue curve), respectively, and implicitly show the unstable domain \mathcal{D}_3 in between. As discussed below, domains \mathcal{D}_2 and \mathcal{D}_3 shown in these figures can be prolonged to the interval $w < 2\sigma$.

C. Extension of the stability diagram to $k < 0$

So far the parameter region \mathcal{D} was explored where $k > 0$, which is constituted by domains \mathcal{D}_1 , \mathcal{D}_2 , and \mathcal{D}_3 . Domain

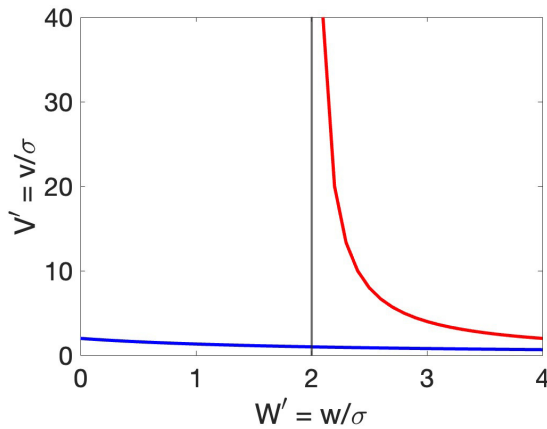


FIG. 6. Curves $V' = \Gamma^2/(W' \pm 2)$ representing boundaries (17) for $\sigma = 1.0$ and $g = 2.0$, in terms of dimensionless variables $V' = v/\sigma$, $W' = w/\sigma$, and $\Gamma = g/\sigma$. The comparison with Fig. 5 shows how reducing g implies that the lower blue boundary tends to a horizontal axis with the collapse of the stability domain \mathcal{D}_2 . In parallel, the upper red boundary approaches the asymptote $W' = 2$. As a consequence, \mathcal{D}_3 , the unstable domain, reduces to a vertical rectangular region with basis $0 < W' < 2$ while \mathcal{D}_1 , the stable domain, becomes the region with $2 < W' < \infty$, $V' > 0$.

\mathcal{D} can be extended to include the region $k = w - 2\sigma < 0$. This circumstance implies a structural change of the initial Hamiltonian (3) which takes the form

$$H = \frac{v}{2}P^2 - \frac{|k|}{2}p^2 + \frac{u}{2}x^2 + \frac{v}{2}X^2 + g(xX + pP), \quad (18)$$

where the change of the k sign causes a negative kinetic-energy-like contribution. By implementing the diagonalization process based on transformation $U = S_{\theta}D_{\alpha}R_{\phi}$, the diagonal Hamiltonian is found to be

$$\mathbb{H}_3 = \frac{q}{4}(P^2 - p^2) + \frac{v_-}{4q}x^2 + \frac{v_+}{4q}X^2, \quad (19)$$

whose parameters can be shown to have the form

$$q = 2\sqrt{g^2 + v|k|}, \quad v_{\pm} = \sqrt{G} \pm \delta, \quad \delta = 2(v^2 - u|k| + 2g^2),$$

and

$$G = 2[(v^2 + u|k|)^2 + 4g^2(v + u)(v - |k|)].$$

The process leading to the diagonal form (19) is discussed in Appendix D. Hamiltonian (19) exhibits an inverted harmonic oscillator for

$$v_- > 0 \rightarrow v > f_+(w) = \frac{g^2}{w + 2\sigma},$$

a condition showing how the same curve characterizing the (blue) lower boundary of the instability regime associated with the domain \mathcal{D}_3 can be extended to the interval $0 < w < 2\sigma$. The presence of the asymptote at $w = 2\sigma$, shows how the infinite stripe corresponding to $f_+(w) < v < \infty$ based on the interval $0 < w < 2\sigma$ constitutes the extension of \mathcal{D}_3 . On the other hand, the violation of inequality $v > f_+(w)$ implies that $v_- < 0$ so that in Hamiltonian (19) the inverted harmonic oscillator becomes a harmonic oscillator. Then, below curve $f_+(w)$ a stability region is found which represents the prolongation of the stability domain \mathcal{D}_2 . This extension is well visible in Figures 1, 3, 5, and 6.

III. SPECTRAL PROPERTIES

The changes in the energy-spectrum structure of H in the transition from \mathcal{D}_1 or \mathcal{D}_2 to \mathcal{D}_3 are the hallmark of the onset of an unstable behavior. In \mathcal{D}_1 , the spectrum of H is obtained from that of Hamiltonian (10), as they are unitarily equivalent. The spectrum is formed by two contributions related to the oscillator sub-Hamiltonians H_{xp} and H_{Xp} (depending on x, p and X, P , respectively) such that $H_3 = H_{xp} + H_{Xp}$. Then, the relevant eigenvalues have the form

$$E(n, m) = \Omega_+ n + \Omega_- m, \quad n, m \in \mathbb{N}_0 \quad (20)$$

(\mathbb{N}_0 the set of positive integers including zero) where the frequencies

$$\Omega_{\pm} = \frac{1}{2} \sqrt{\Delta \pm \frac{1}{2\rho} \sqrt{D^2 + 4A^2}}$$

depend on the model parameters through the quantities ρ, A, D , and Δ . By approaching the lower boundary $v = g^2/(w - 2\sigma)$ of \mathcal{D}_1 from above one finds that

$$\Delta \rightarrow \frac{1}{2\rho} \sqrt{D^2 + 4A^2} \Rightarrow \Omega_- \rightarrow 0^+,$$

showing how the variation of quantum number n is associated to the large-scale energy changes while m describes the fine structure of the spectrum since Ω_- implies a vanishingly small interlevel separation. This behavior represents the spectral collapse [30] corresponding, at the classical level, to the transition to an unstable dynamical regime. Quantum mechanically, it precludes the occurrence of a continuous spectrum which will be associated with the domain \mathcal{D}_3 . Within this domain Hamiltonian (16) is equipped with the XP sub-Hamiltonian

$$\mathcal{H}_{XP} = \frac{\eta}{4}P^2 - \frac{\tau_-}{4\eta}X^2, \quad \tau_- = \sqrt{B} - \chi > 0,$$

which is unitarily equivalent, up to a constant factor, to $P^2 - X^2$. The latter, one of the noncompact generators of $\mathfrak{su}(1,1)$, is known to exhibit a continuous spectrum whose eigenstates are the Lindblad-Nagel states [37,38]. The energy spectrum of Hamiltonian (16) is thus given by

$$E'(n, \Lambda) = \omega_+ n + \omega_- \Lambda, \quad \omega_{\pm} = \frac{1}{2}\sqrt{\sqrt{B} \pm \chi},$$

exhibiting a discrete part parametrized by $n \in \mathbb{N}_0$, and a continuous part parametrized by $\Lambda \in \mathbb{R}$. Such spectral properties are easily extended to Hamiltonian (19) due to its similarity with Hamiltonian (16). Crossing the lower boundary $v = g^2/(w + 2\sigma)$ of \mathcal{D}_3 one reaches the stable domain \mathcal{D}_2 where \mathcal{H}_3 is formed by two harmonic oscillators since in this region of \mathcal{D} one has $\chi \pm \sqrt{B} > 0$. The resulting spectrum

$$E'(n, m) = W_+ n + W_- m, \quad W_{\pm} = \frac{1}{2}\sqrt{\chi \pm \sqrt{B}}$$

is discrete and features the expected transition to a continuous distribution of energy levels when $W_- \rightarrow 0$. This collapse takes place for $\sqrt{B} \rightarrow \chi$, a limit case causing the approach from below to the upper boundary $v = g^2/(w + 2\sigma)$ of domain \mathcal{D}_2 .

IV. TIME EVOLUTION AND AVERAGE POPULATION OF MODES a AND b

The time evolution of the expectation values of number operators $a^\dagger a$ and $b^\dagger b$ provides a second way to characterize stable and unstable regimes. We then calculate these quantities by using well-known semiclassical states, the Weyl-Heisenberg (or Glauber) coherent states (see, e.g., Ref. [39]). These are defined by

$$a|\alpha\rangle = \alpha|\alpha\rangle \rightarrow |\alpha\rangle = e^{-|\alpha|^2/2} \sum_{n=0}^{\infty} \frac{\alpha^n}{\sqrt{n!}} |n\rangle, \quad (21)$$

where $|n\rangle$ are number states satisfying $a^\dagger |n\rangle = n|n\rangle$ and $\alpha \in \mathbb{C}$. Likewise, coherent states $|\beta\rangle$ can be defined for mode b which satisfy equation $b|\beta\rangle = \beta|\beta\rangle$ with $\beta \in \mathbb{C}$. The time evolution of $\langle a^\dagger a \rangle_t$ is described by

$$\langle a^\dagger a \rangle_t = \langle \beta, \alpha | P_t^\dagger a^\dagger a P_t | \alpha, \beta \rangle, \quad P_t = e^{-itH/\hbar}, \quad (22)$$

where $P_t | \alpha, \beta \rangle$ are solutions to the Schrödinger equation and the initial state is a product coherent state $|\alpha, \beta\rangle = |\alpha\rangle |\beta\rangle$. To highlight the different dynamical behavior that characterizes the three domains \mathcal{D}_i , $i = 1, 2, 3$ of the stability diagram, we adopt the Heisenberg-picture viewpoint and calculate the operator evolution $P_t^\dagger a^\dagger a P_t$ and $P_t^\dagger b^\dagger b P_t$.

A. Time evolution of the mode populations in the stability regimes

Here, one considers the stability regime relevant to domain \mathcal{D}_1 defined by Eq. (12). After observing that $H = U^\dagger H_3 U$, this amounts to implementing the transformation

$$\begin{aligned} P_t^\dagger a P_t &= e^{-itH} a e^{-itH} = U^\dagger e^{-itH_3} U a U^\dagger e^{-itH_3} U \\ &= \frac{1}{\sqrt{2}} U^\dagger e^{-itH_3} U (x + ip) U^\dagger e^{-itH_3} U. \end{aligned} \quad (23)$$

In the domain \mathcal{D}_1 the diagonal Hamiltonian H_3 is given by formula (10) and $U = R_\mu D_\alpha R_\phi$. Because of their complexity, the intermediate steps of the calculation of $a_t = P_t^\dagger a P_t$ are reported in Appendix A. The derivation of (23) provides a linear combination of x , p , X , and P which, expressed in terms of operators a , a^\dagger , b , and b^\dagger , reads

$$a_t = \frac{1}{2}(f_{13}^- a + f_{13}^+ a^\dagger + f_{24}^- b + f_{24}^+ b^\dagger). \quad (24)$$

The time-dependent coefficients f_{13}^\pm and f_{24}^\pm have the form

$$\begin{aligned} f_{13}^\pm &= f_1 \pm i f_3 = (1 \mp 1)(A_1 A_2 C_t^+ + A_3 A_4 C_t^-) \\ &\quad - i \left(\frac{A_2^2}{r_+} \mp r_+ A_1^2 \right) S_t^+ - i \left(\frac{A_4^2}{r_-} \mp r_- A_3^2 \right) S_t^-, \\ f_{24}^\pm &= f_2 \pm i f_4 = (A_1 A_3 \mp A_2 A_4)(C_t^- - C_t^+) \\ &\quad + i \left(\frac{A_2 A_3}{r_+} \mp r_+ A_1 A_4 \right) S_t^+ - i \left(\frac{A_4 A_1}{r_-} \mp r_- A_3 A_2 \right) S_t^-, \end{aligned}$$

where

$$C_t^\pm = \cos\left(\frac{t}{2}\sqrt{\sigma_\pm}\right), \quad S_t^\pm = \sin\left(\frac{t}{2}\sqrt{\sigma_\pm}\right), \quad (25)$$

and coefficients f_1 , f_2 , f_3 , and f_4 are derived in Appendix A. The effect of transformation U is incorporated in A_i , $i = 1, 2, 3, 4$ [see formulas (A3) and (A4)]. By recalling that the coherent-state definitions (21) entails $\langle \alpha | a | \alpha \rangle = \alpha$ and $\langle \alpha | a^\dagger a | \alpha \rangle = |\alpha|^2$ (similar formulas hold for b and b^\dagger by using state $|\beta\rangle$), then the expectation value (22) of the number operator $a^\dagger a$ provided by the time-evolved state $P_t | \alpha, \beta \rangle$ is found to be

$$\begin{aligned} \langle a^\dagger a \rangle_t &= \langle \beta, \alpha | a_t^\dagger a_t | \alpha, \beta \rangle \\ &= C_0 + \frac{1}{4} |f_{13}^- \alpha + f_{13}^+ \alpha^* + f_{24}^- \beta + f_{24}^+ \beta^*|^2 \end{aligned} \quad (26)$$

with $C_0 = (|f_{13}^+|^2 + |f_{24}^+|^2)/4$. The dependence on time caused by the trigonometric functions S_t^\pm and C_t^\pm shows how, despite the complexity of parameters f_{13}^\pm and f_{24}^\pm , in this regime the time-dependent average population (26) exhibits periodic oscillations. This behavior is illustrated in Fig. 2. The same conclusion is found when calculating $\langle b^\dagger b \rangle_t$, its evolution being dependent on time-periodic parameters (25).

Appendix B provides the derivation of the expectation value $\langle a^\dagger a \rangle_t$ (and, implicitly, of $\langle b^\dagger b \rangle_t$) in the stability regime relevant to domain \mathcal{D}_2 defined by Eq. (15). These are shown to exhibit the same regular oscillations characterizing domain \mathcal{D}_1 .

B. Time evolution of the mode populations in the instability regime

A significant change in the evolution of populations $\langle a^\dagger a \rangle_t$ and $\langle b^\dagger b \rangle_t$ crops up in the instability regime relevant to \mathcal{D}_3 . The condition $\sqrt{B} - \chi > 0$ characterizing this regime dramatically affects the time behavior of

$$a_t = P_t^\dagger a P_t = U^\dagger e^{-it\mathcal{H}_3} U a U^\dagger e^{-it\mathcal{H}_3} U, \quad (27)$$

since Hamiltonian (14) takes the form

$$\mathcal{H}_3 = \frac{\eta}{4} p^2 + \frac{\tau_\pm}{4\eta} x^2 - \left(\frac{\eta}{4} p^2 - \frac{\tau_\pm}{4\eta} X^2 \right), \quad (28)$$

with $\tau_\pm = |\sqrt{B} \pm \chi|$ and $\eta = 2\sqrt{g^2 - kv}$ [see Eq. (14)], showing the presence of an inverted harmonic oscillator. The resulting time-dependent transformations

$$V_t x V_t^\dagger = x C_t^+ + p R_+ S_t^+, \quad V_t p V_t^\dagger = p C_t^+ - \frac{x}{R_+} S_t^+,$$

$$V_t X V_t^\dagger = X C_t^- - P R_- S_t^-, \quad V_t P V_t^\dagger = P C_t^- + \frac{X}{R_-} S_t^-,$$

where

$$V_t = e^{it\mathcal{H}_3}, \quad R_\pm = \sqrt{\eta^2/\tau_\pm}$$

involve time-dependent periodic functions

$$C_t^+ = \cos\left(\frac{t}{2}\sqrt{\tau_+}\right), \quad S_t^+ = \sin\left(\frac{t}{2}\sqrt{\tau_+}\right),$$

but also time-dependent hyperbolic functions

$$C_t^- = \cosh\left(\frac{t}{2}\sqrt{\tau_-}\right), \quad S_t^- = \sinh\left(\frac{t}{2}\sqrt{\tau_-}\right), \quad (29)$$

caused by the inverted oscillator contained in \mathcal{H}_3 . This term, including a noncompact generator of algebra $\text{Sp}(4)$, triggers diverging behaviors in the evolution of the expectation values $\langle a^\dagger a \rangle_t$ and $\langle b^\dagger b \rangle_t$. The derivation of the time-evolved mode $a_t = P_t^\dagger a P_t$, discussed in Appendix C, gives the evolution of the relevant mode population

$$\begin{aligned} \langle a^\dagger a \rangle_t &= \langle \beta, \alpha | P_t^\dagger a^\dagger a P_t | \alpha, \beta \rangle = \langle \beta, \alpha | a_t^\dagger a_t | \alpha, \beta \rangle \\ &= C_0(t) + \frac{1}{4} |G_{13}^- \alpha + G_{13}^+ \alpha^* + G_{24}^- \beta + G_{24}^+ \beta^*|^2 \end{aligned} \quad (30)$$

with $C_0(t) = \frac{1}{4} (|G_{13}^+|^2 + |G_{24}^+|^2)$ and

$$\begin{aligned} G_{13}^\pm &= G_1 \pm iG_3 = (1 \mp 1)(B_1 B_2 C_t^+ + B_3 B_4 C_t^-) \\ &\quad - i \left(\frac{B_2^2}{R_+} \mp R_+ B_1^2 \right) S_t^+ - i \left(\frac{B_4^2}{R_-} \mp R_- B_3^2 \right) S_t^-, \\ G_{24}^\pm &= G_2 \pm iG_4 = (B_1 B_3 \mp B_2 B_4)(C_t^- - C_t^+) \\ &\quad + i \left(\frac{B_2 B_3}{R_+} \mp R_+ B_1 B_4 \right) S_t^+ - i \left(\frac{B_4 B_1}{R_-} \mp R_- B_3 B_2 \right) S_t^-, \end{aligned}$$

where G_1, G_2, G_3 , and G_4 are defined in Appendix C, and coefficients B_i , $i = 1, 2, 3, 4$, describe the effect of transformation $U = S_\theta D_\alpha R_\phi$ on x, p, X , and P [see Eqs. (B1) and (B2)]. Formula (30) shows that, for any $\alpha, \beta \neq 0$, one finds $\langle a^\dagger a \rangle_t = |\alpha|^2$ at $t = 0$. For large t , G_{13}^\pm and G_{24}^\pm are dominated by $e^{\sqrt{\tau_\pm} t}$ describing the amplification effect one naturally associates to the unstable regime. This behavior is illustrated in Fig. 4. Interestingly, when the initial mode populations are

assumed to be zero, meaning that $\langle a^\dagger a \rangle_0 = C_0(0) = 0$ due to $\alpha = 0$ and $\beta = 0$, for t large enough,

$$\langle a^\dagger a \rangle_t = C_0(t) = \text{const} \times e^{\sqrt{\tau_-} t}$$

showing how the term C_0 is sufficient to trigger the amplification effect. Similar behaviors can be shown to characterize the second-mode population $\langle b^\dagger b \rangle_t$ for $t = 0$ and sufficiently large t .

It is worth mentioning that this diverging behavior is well known within quantum optics, where the degenerate PDC is associated to the amplification effect, namely, the increasing of the mode photon number. Its physical interpretation is related to the presence of an intense pump mode which can be treated semiclassically [22]. The experimental detection of this effect can be done through photodetectors which measure the output radiation intensity. As for boson models described in the BH picture, one readily recognizes that the role of the pump mode is played by the macroscopically occupied ground-state mode which becomes a semiclassical observable [28].

V. DISCUSSION

Figures 1, 3, 5, and 6 describe the stability diagram \mathcal{D} of model (1) as a function of frequencies v and w for different choices of the interaction parameter g and of the amplification parameter σ . In all cases an instability domain \mathcal{D}_3 , featuring the amplification effect, appears which separates the stability domains \mathcal{D}_1 and \mathcal{D}_2 where the expectation values of modes' populations exhibit an oscillatory behavior. The discussion in Sec. II C shows how \mathcal{D} can be extended to the entire quadrant $w, v > 0$.

In general, all figures clearly show the role played by the interaction g . To highlight this effect, with reference, for example, to Fig. 1 and to $v = f_-(w)$ [see formulas (17)], one can consider a horizontal line associated with a given value v . Moving along this line, one easily recognizes a semi-infinite stability interval $w > \bar{w}$, with $\bar{w} = 2\sigma + g^2/v$ (the intersection point of the $v = \text{const}$ line with the red boundary), and a finite interval $0 < w < \bar{w}$ where the amplification effect takes place. Note that this interval is larger than that of the $g = 0$ case, being $2\sigma < \bar{w}$. This is the first effect caused by the interaction. A second, more surprising effect due to $g \neq 0$ appears when $v < f_+(0) = g^2/(2\sigma)$ which corresponds to the emergence of the stable region \mathcal{D}_2 . In this case, the amplification interval along a horizontal line with $v = \text{const}$, becomes $w_* < w < \bar{w}$ where $w_* = g^2/(v - 2\sigma)$ is obtained from $v = f_+(w)$ [see formulas (17)] and represents the intersection point of the $v = \text{const}$ line with the blue boundary. For $0 < w < w_*$ a new stability interval crops up which becomes more and more extended by decreasing v and for $0 < v < f_+(0)$ generates the infinite domain \mathcal{D}_2 bounded from above by $v = f_+(w)$.

The effect of reducing the amplification parameter is shown in Figs. 1 and 3 where the boundaries (17), separating \mathcal{D}_1 and \mathcal{D}_2 from \mathcal{D}_3 , are illustrated for $\sigma = 0.5$ and $\sigma = 0.1$, respectively, and with a fixed interaction parameter $g = 1.0$. Curves $V = F_\pm(W) = 1/(W \pm 2\Sigma)$, representing boundaries (17), are expressed in terms of dimensionless variables $V = v/g$, $W = w/g$, and $\Sigma = \sigma/g$. The comparison of Fig. 1 with

Fig. 3, in which $\Sigma = \sigma/g$ is reduced, highlights the collapse of the instability domain \mathcal{D}_3 for $\Sigma \rightarrow 0$ caused by the approaching of the asymptote at $W = 2$ to the vertical axis with the simultaneous extension of \mathcal{D}_1 and \mathcal{D}_2 . These end up merging in a unique stable domain since the upper boundary $V = F_+(W)$ of \mathcal{D}_2 tends to the lower boundary $V = F_-(W)$ of \mathcal{D}_1 . Accordingly, in this limit, Hamiltonian (1) reduces to an elementary system involving two coupled modes whose stable character is ensured for any choice of parameters w , v , and g . For $\sigma \rightarrow 0$, rotation R_ϕ [see formulas (4) and (5)] is sufficient to take Hamiltonian H_1 of Secs. II A (regime $g^2 < kv$) and II B (regime $g^2 > kv$) into a diagonal form. In both cases, in fact, potential $V(x, X)$ in H_1 loses the coupling term xX since condition $\sigma = 0$ implies $u = k$.

The effect of increasing g is illustrated in Figs. 5 and 6. These describe the behavior of the curves $V' = G_\pm(W') = \Gamma^2/(W' \pm 2)$ representing boundaries (17), for $\sigma = 1.0$, $g = 5.0$, and $g = 2.0$, respectively, in terms of dimensionless variables $V' = v/\sigma$, $W' = w/\sigma$, and $\Gamma = g/\sigma$. Comparing Fig. 5 with Fig. 6 (note that the latter features a smaller g) highlights the collapse of the stability domain \mathcal{D}_2 whose upper (blue) boundary $V' = G_+(W')$ tends to the horizontal axis. In the same limit, one observes that the \mathcal{D}_1 boundary $V' = G_-(W')$ approaches the asymptote $W' = 2$ while for $W' > 2$ it tends to the horizontal axis. Then the unstable domain \mathcal{D}_3 occupies the vertical rectangular region whose basis is the interval $0 < W' < 2$. This scenario well describes the simplified stability diagram associated to Hamiltonian (3) for $g = 0$, where the XP sub-Hamiltonian is always stable while the emergence of the amplification effect is caused by the xp sub-Hamiltonian for $w < 2\sigma$, namely, for $W' < 2$ in Fig. 6. Summarizing, in the limit case $g = 0$ the stability diagram simplifies its structure exhibiting only two regions, an (unstable) amplification region and a stability region characterized by the intervals $0 < w < 2\sigma$ and $\sigma < w < \infty$, respectively, and by $0 < v < \infty$.

VI. CONCLUSIONS

This paper investigates the stability diagram of a two-mode Hamiltonian characterized by the coupling of modes where one of the two modes undergoes the effect of a quadratic amplification. The stability diagram reveals a novel structure determined by the reciprocal influence of the interaction and amplification parameters g and σ .

In Sec. II, the dynamical-algebra method is implemented to reduce the model Hamiltonian into a diagonal form. This allows one to recognize the stable and unstable regions associated to the presence of standard and inverted harmonic oscillators, respectively, in the diagonal Hamiltonian. This analysis leads to the definition of the stability diagram described in Figs. 1–6.

The changes in spectral structure of the model Hamiltonian, discussed in Sec. III, when crossing the borders separating stable and unstable regions represent a significant signature of the transition from a stable (discrete spectrum) to an unstable (continuous spectrum) behavior. Section IV supplies a further independent confirmation of the information encoded in the stability diagram. In particular, the expectation value of the number operators of both modes (describing the average mode populations) exhibit oscillatory time evolution

in stable regimes while unstable regimes feature an exponentially diverging behavior when the interplay between g and σ allows the amplification effect to crop up.

Section V highlights the role played by parameters g and σ in the stability diagram. More specifically, Figs. 1 and 3 show how reducing σ determines the collapse of the unstable domain \mathcal{D}_3 with the parallel merging of domains \mathcal{D}_1 and \mathcal{D}_2 in a unique stable region. On the other hand, Figs. 5 and 6 show the collapse of \mathcal{D}_2 reproducing the simpler stability diagram of two independent modes ($g = 0$). In particular, the resulting stability diagram, which for $g = 0$ exhibits a stable region and an unstable amplification region controlled by σ , for $g \neq 0$, features an unexpected splitting of the unstable amplification region into two subregions, one of which exhibits a stable character and an extension controlled by the interaction g .

On the theoretical side, the dynamical-algebra method applied in this paper and the ensuing analysis leading to the identification of stable and unstable regimes can be applied to many physical systems. For example, the Dicke model of quantum optics and the two-mode models describing bosonic mixtures confined in two potential wells. On the other hand, from the experimental point of view, a quantum-optical system with two-mode coupling can be equipped with a semiclassical pump mode resulting in the degenerate PDC in which the amplification term of model (1) is embedded. Likewise, Bose-Hubbard-like systems, whose realization is well known within ultracold atom physics [40], reveal amplification terms when implementing the Bogoliubov approximation [28]. Therefore, the results highlighted in this paper suggest the exploration of a phenomenology which seems to be accessible to the current experimental techniques.

ACKNOWLEDGMENTS

The authors wish to thank M. Genovese for enlightening comments about the mechanism and the measurement schemes characterizing the parametric amplifiers.

APPENDIX A: MODE-POPULATION EVOLUTION IN THE STABILITY REGIME WITH $g^2 < kv$

To determine the time evolution of the expectation value of the mode- a population $\langle a^\dagger a \rangle_t$ in the parameter region corresponding to domain \mathcal{D}_1 one must calculate Eq. (23), namely,

$$a_t = P_t^\dagger a P_t = \frac{1}{\sqrt{2}} U^\dagger e^{iH_3} U(x + ip) U^\dagger e^{-iH_3} U,$$

where $U = R_\mu D_\alpha R_\phi$; we exploit Eqs. (4)–(7) finding

$$UxU^\dagger = A_1x + A_3X, \quad UpU^\dagger = A_2p + A_4P, \quad (A1)$$

$$UXU^\dagger = A_2X - A_4x, \quad UPU^\dagger = A_1P - A_3p, \quad (A2)$$

with

$$A_1 = cCe^\alpha - sSe^{-\alpha}, \quad A_2 = cCe^{-\alpha} - sSe^\alpha, \quad (A3)$$

$$A_3 = cSe^\alpha + sCe^{-\alpha}, \quad A_4 = cSe^{-\alpha} + sCe^\alpha, \quad (A4)$$

and $c = \cos \phi$, $s = \sin \phi$, $C = \cos \mu$, $S = \sin \mu$. Parameter α is defined by Eq. (9). Due to the unitary character of U

the equation $A_1A_2 + A_3A_4 = 1$ is satisfied. The corresponding inverse transformations read

$$U^\dagger xU = A_2x - A_3X, \quad U^\dagger pU = A_1p - A_4P, \quad (\text{A5})$$

$$U^\dagger XU = A_1X + A_4x, \quad U^\dagger PU = A_2P + A_3p, \quad (\text{A6})$$

while the time-dependent transformation generated by H_3 gives the time-evolved operators

$$W_t x W_t^\dagger = x C_t^+ + p r_+ S_t^+, \quad W_t p W_t^\dagger = p C_t^+ - \frac{x}{r_+} S_t^+,$$

$$W_t X W_t^\dagger = X C_t^- + P r_- S_t^-, \quad W_t P W_t^\dagger = P C_t^- - \frac{X}{r_-} S_t^-,$$

where $W_t = e^{iH_3 t}$ and the Hamiltonian (10) has been rewritten as

$$H_3 = \frac{\gamma}{4} p^2 + \frac{\sigma_+}{4\gamma} x^2 + \frac{\gamma}{4} P^2 + \frac{\sigma_-}{4\gamma} X^2.$$

The time-dependent terms have the form

$$C_t^\pm = \cos\left(\frac{t}{2}\sqrt{\sigma_\pm}\right), \quad S_t^\pm = \sin\left(\frac{t}{2}\sqrt{\sigma_\pm}\right),$$

and

$$r_\pm = \sqrt{\gamma^2/\sigma_\pm}, \quad \sigma_\pm = \Delta \pm \frac{1}{2\rho}\sqrt{D^2 + 4A^2}.$$

By combining such formulas one finds the linear combination

$$a_t = P_t^\dagger a P_t = \frac{1}{\sqrt{2}}(f_1(t)x + f_2(t)X + f_3(t)p + f_4(t)P),$$

where

$$f_1(t) = A_1A_2C_t^+ + A_3A_4C_t^- - i\frac{A_2^2}{r_+}S_t^+ - i\frac{A_4^2}{r_-}S_t^-,$$

$$f_2(t) = A_1A_3(C_t^- - C_t^+) + i\frac{A_2A_3}{r_+}S_t^+ - i\frac{A_4A_1}{r_-}S_t^-,$$

$$f_3(t) = A_1^2 r_+ S_t^+ + A_3^2 r_- S_t^- + iA_1A_2C_t^+ + iA_4A_3C_t^-,$$

$$f_4(t) = A_3A_2r_-S_t^- - A_1A_4r_+S_t^+ + iA_2A_4(C_t^- - C_t^+).$$

Formula (24) provides a_t in terms of operators a , a^\dagger , b , and b^\dagger and of coefficients $f_{13}^\pm = f_1 \pm if_3$ and $f_{24}^\pm = f_2 \pm if_4$. The same procedure allows us to evaluate the time evolution of the expectation value $\langle b^\dagger b \rangle_t$, relevant to the population of mode b . One finds

$$b_t = \frac{1}{2}(F_{13}^- b + F_{13}^+ b^\dagger + F_{24}^- a + F_{24}^+ a^\dagger), \quad (\text{A7})$$

with time-dependent coefficients F_{13}^\pm and F_{24}^\pm given by

$$F_{13}^\pm = F_1 \pm iF_3 = (1 \mp 1)(A_1A_2C_t^- + A_3A_4C_t^+) - i\left(\frac{A_1^2}{r_-} \pm r_-A_2^2\right)S_t^- - i\left(\frac{A_3^2}{r_+} \pm r_+A_4^2\right)S_t^+,$$

$$F_{24}^\pm = F_2 \pm iF_4 = (A_2A_4 \pm A_1A_3)(C_t^- - C_t^+) - i\left(\frac{A_2A_3}{r_+} \mp r_+A_1A_4\right)S_t^+ - i\left(\frac{A_1A_4}{r_-} \pm r_-A_2A_3\right)S_t^-.$$

The similarity of formulas (24) and (A7) implies the expected result that, in the stability domain \mathcal{D}_1 , also the b -mode population features regular oscillations.

APPENDIX B: MODE-POPULATION EVOLUTION IN THE STABILITY REGIME WITH $g^2 > kv$

We consider the expectation value $\langle a^\dagger a \rangle_t$ describing the mode- a population relevant to the stability domain \mathcal{D}_2 where Hamiltonian (14) satisfies the stability condition $\sqrt{B} - \chi < 0$. Its time evolution is easily found by repeating the calculation scheme applied in Appendix A. To calculate

$$a_t = P_t^\dagger a P_t = \frac{1}{\sqrt{2}}U^\dagger e^{i\mathcal{H}_3 t} U(x + ip)U^\dagger e^{-i\mathcal{H}_3 t} U$$

we exploit the transformation

$$UxU^\dagger = B_1x + B_3X, \quad UpU^\dagger = B_2p + B_4P,$$

$$UXU^\dagger = B_2X - B_4x, \quad UPU^\dagger = B_1P - B_3p,$$

with $U = S_\theta D_\alpha R_\phi$,

$$B_1 = cCe^\alpha + sSe^{-\alpha}, \quad B_2 = cCe^{-\alpha} - sSe^\alpha, \quad (\text{B1})$$

$$B_3 = cSe^\alpha + sCe^{-\alpha}, \quad B_4 = sCe^\alpha - cSe^{-\alpha}, \quad (\text{B2})$$

and $c = \cos \phi$, $s = \sin \phi$, $C = \cosh \theta$, $S = \sinh \theta$. Parameter α is defined by Eq. (13) while θ , given by

$$\tanh(2\theta) = \frac{8g|k - u|\sqrt{g^2 - kv}}{2\rho^2(w + v) + (k^2 - v^2)(u - k)}, \quad (\text{B3})$$

allows one to remove the coupling term xX in Hamiltonian (14). The unitary character of U entails that equation $B_1B_2 + B_3B_4 = 1$ is satisfied. The corresponding inverse transformations $U^\dagger QU$ with $Q = x, p, X, P$ are easily found by means of the substitutions $A_i \rightarrow B_i$, $i = 1, 2, 3, 4$ in Eqs. (A5) and (A6). In the current regime, where the condition $\sqrt{B} - \chi < 0$ is satisfied, Hamiltonian (14) is written as

$$\mathcal{H}_3 = \frac{\eta}{4} p^2 + \frac{\tau_+}{4\eta} x^2 - \left(\frac{\eta}{4} P^2 + \frac{\tau_-}{4\eta} X^2\right),$$

with $\tau_\pm = |\sqrt{B} \pm \chi|$, and generates the time-dependent transformations

$$U_t x U_t^\dagger = x C_t^+ + p R_+ S_t^+, \quad U_t p U_t^\dagger = p C_t^+ - \frac{x}{R_+} S_t^+,$$

$$U_t X U_t^\dagger = X C_t^- - P R_- S_t^-, \quad U_t P U_t^\dagger = P C_t^- + \frac{X}{R_-} S_t^-,$$

where

$$U_t = e^{i\mathcal{H}_3 t}, \quad R_\pm = \sqrt{\eta^2/\tau_\pm},$$

and parameters

$$C_t^\pm = \cos\left(\frac{t}{2}\sqrt{\tau_\pm}\right), \quad S_t^\pm = \sin\left(\frac{t}{2}\sqrt{\tau_\pm}\right)$$

take into account the dependence on time. As in the stability regime corresponding to \mathcal{D}_1 with $g^2 < kv$, these formulas allow us to calculate the time-evolved operator $a_t = (g_1x + g_2X + g_3p + g_4P)/\sqrt{2}$, which, expressed in terms of a , a^\dagger , b ,

and b^\dagger , reads

$$a_t = \frac{1}{2}(g_{13}^- a + g_{13}^+ a^\dagger + g_{24}^- b + g_{24}^+ b^\dagger),$$

where

$$\begin{aligned} g_{13}^\pm &= g_1 \pm ig_3 = (1 \mp 1)(B_1 B_2 C_t^+ + B_3 B_4 C_t^-) \\ &\quad - i \left(\frac{B_2^2}{r_+} \mp r_+ B_1^2 \right) S_t^+ + i \left(\frac{B_4^2}{r_-} \mp r_- B_3^2 \right) S_t^-, \\ g_{24}^\pm &= g_2 \pm ig_4 = (B_1 B_3 \mp B_2 B_4)(C_t^- - C_t^+) \\ &\quad + i \left(\frac{B_2 B_3}{r_+} \mp r_+ B_1 B_4 \right) S_t^+ + i \left(\frac{B_4 B_1}{r_-} \mp r_- B_3 B_2 \right) S_t^-. \end{aligned}$$

The expectation value of the number operator $\langle a^\dagger a \rangle_t = \langle \alpha, \beta | a_t^\dagger a_t | \alpha, \beta \rangle$ for an initial state corresponding to a product coherent state $|\alpha, \beta\rangle$ is easily found by repeating the calculations shown in Appendix A for the stability regime relevant to \mathcal{D}_1 . Not surprisingly, even in the present case (the stability regime relevant to \mathcal{D}_2) the population of mode a features regular oscillations since ξ_{13}^\pm and ξ_{24}^\pm are simple linear combinations of C_t^\pm and S_t^\pm . These conclusions are easily extended to the b -mode population $\langle b^\dagger b \rangle_t$.

APPENDIX C: MODE EVOLUTION IN THE INSTABILITY REGIME

The condition $\sqrt{B} - \chi > 0$ characterizes the instability regime in which Hamiltonian (28) includes an inverted harmonic oscillator. The calculation of $V_t x V_t^\dagger$, $V_t p V_t^\dagger$, $V_t X V_t^\dagger$, and $V_t P V_t^\dagger$ where $V_t = e^{i\mathcal{H}_3}$ (see Sec. IV B), allows one, in turn, to calculate

$$a_t = P_t^\dagger a P_t = \frac{1}{\sqrt{2}} U^\dagger e^{i\mathcal{H}_3} U (x + ip) U^\dagger e^{-i\mathcal{H}_3} U.$$

We find $a_t = (G_1 x + G_2 X + G_3 p + G_4 P) / \sqrt{2}$ which depends on time through the parameters

$$\begin{aligned} G_1(t) &= B_1 B_2 C_t^+ + B_3 B_4 C_t^- - i \frac{B_2^2}{R_+} S_t^+ + i \frac{B_4^2}{R_-} S_t^-, \\ G_2(t) &= B_1 B_3 (C_t^- - C_t^+) + i \frac{B_2 B_3}{R_+} S_t^+ + i \frac{B_4 B_1}{R_-} S_t^-, \\ G_3(t) &= B_1^2 R_+ S_t^+ - B_3^2 R_- S_t^- + i B_1 B_2 C_t^+ + i B_4 B_3 C_t^-, \\ G_4(t) &= -B_3 B_2 R_- S_t^- - B_1 B_4 R_+ S_t^+ + i B_2 B_4 (C_t^- - C_t^+). \end{aligned}$$

This enables one to derive in Sec. IV B the expectation value $\langle a^\dagger a \rangle_t$ expressed in terms of parameters $G_{13}^\pm = G_1 \pm iG_3$ and $G_{24}^\pm = G_2 \pm iG_4$.

APPENDIX D: EXTENSION OF THE INSTABILITY REGIME TO $w < 2\sigma$

This regime features $k = w - 2\sigma < 0$, a circumstance implying that the initial Hamiltonian has the form

$$H = \frac{v}{2} p^2 - \frac{|k|}{2} p^2 + \frac{u}{2} x^2 + \frac{v}{2} X^2 + g(xX + pP). \quad (D1)$$

This reduces to

$$\mathbb{H}_3 = \frac{q}{4}(P^2 - p^2) + \frac{v_-}{4q} x^2 + \frac{v_+}{4q} X^2, \quad (D2)$$

with

$$2q = \sqrt{g^2 + v|k|}, \quad v_\pm = \sqrt{G} \pm \delta, \quad \delta = 2(v^2 - u|k| + 2g^2),$$

and

$$G = 2[(v^2 + u|k|)^2 + 4g^2(v + u)(v - |k|)],$$

by implementing the transformation $U = S_\theta D_\alpha R_\phi$. The diagonal form \mathcal{H}_3 is achieved for ϕ , α , and θ by satisfying the conditions

$$\tan(2\phi) = \frac{2g}{|k| + v}, \quad e^{2\alpha} = \sqrt{\frac{R + |k| - v}{R + v - |k|}}, \quad \tanh(2\theta) = -\frac{D}{A},$$

where

$$R = \sqrt{(v + |k|)^2 + 4g^2}, \quad D = 8g(u + |k|)\sqrt{v|k| + g^2},$$

$$A = (2v + u - |k|)R^2 - (v^2 - |k|^2)(u + |k|).$$

Hamiltonian (D2) exhibits an inverted harmonic oscillator for

$$v_- > 0 \rightarrow v > \frac{g^2}{w + 2\sigma},$$

a condition showing how the unstable domain \mathcal{D}_3 can be extended to the interval $0 < w < 2\sigma$. When $v_- > 0$ is violated the inverted harmonic oscillator in Hamiltonian (D2) reduces to the usual harmonic oscillator, and the transition to a stability region takes place.

As in the previous cases, the calculation of the average mode population $\langle a^\dagger a \rangle_t$ is performed by exploiting the Heisenberg picture. From

$$UxU^\dagger = C_1x + C_3X, \quad UpU^\dagger = C_2p + C_4P,$$

$$UXU^\dagger = C_2X - C_4x, \quad UPU^\dagger = C_1P - C_3p,$$

with $U = S_\theta D_\alpha R_\phi$,

$$C_1 = cCe^\alpha + sSe^{-\alpha}, \quad C_2 = cCe^{-\alpha} - sSe^\alpha, \quad (D3)$$

$$C_3 = cSe^\alpha + sCe^{-\alpha}, \quad C_4 = sCe^\alpha - cSe^{-\alpha}, \quad (D4)$$

and $c = \cos\phi$, $s = \sin\phi$, $C = \cosh\theta$, $S = \sinh\theta$, and the time-dependent transformations

$$W_t X W_t^\dagger = X C_t^+ + P R_+ S_t^+, \quad W_t P W_t^\dagger = P C_t^+ - \frac{X}{R_+} S_t^+,$$

$$W_t x W_t^\dagger = x C_t^- - p R_- S_t^-, \quad W_t P W_t^\dagger = p C_t^- + \frac{x}{R_-} S_t^-,$$

where

$$W_t = e^{i\mathcal{H}_3}, \quad R_\pm = \sqrt{q^2/v_\pm},$$

with parameters

$$C_t^- = \cosh\left(\frac{t}{2}\sqrt{v_-}\right), \quad S_t^- = \sinh\left(\frac{t}{2}\sqrt{v_-}\right),$$

$$C_t^+ = \cos\left(\frac{t}{2}\sqrt{v_+}\right), \quad S_t^+ = \sin\left(\frac{t}{2}\sqrt{v_+}\right),$$

one calculates

$$a_t = \frac{1}{\sqrt{2}}U^\dagger W_t U(x + ip)U^\dagger W_t^\dagger U,$$

giving $a_t = \frac{1}{\sqrt{2}}(E_1x + E_2X + E_3p + E_4P)$ with

$$E_1(t) = C_1C_2C_t^- + C_3C_4C_t^+ + i\frac{C_2^2}{R_-}S_t^- - i\frac{C_4^2}{R_+}S_t^+,$$

$$E_2(t) = C_1C_3(C_t^+ - C_t^-) - i\frac{C_2C_3}{R_-}S_t^- - i\frac{C_4C_1}{R_+}S_t^+,$$

$$E_3(t) = C_3^2R_+S_t^+ - C_1^2R_-S_t^- + iC_1C_2C_t^- + iC_4C_3C_t^+,$$

$$E_4(t) = C_3C_2R_+S_t^+ + C_1C_4R_-S_t^- + iC_2C_4(C_t^+ - C_t^-).$$

-
- [1] M. Leib *et al.*, *New J. Phys.* **14**, 075024 (2012).
- [2] S. Schmidt, D. Gerace, A. A. Houck, G. Blatter, and H. E. Türeci, *Phys. Rev. B* **82**, 100507(R) (2010).
- [3] T. E. Lee and M. C. Cross, *Phys. Rev. A* **88**, 013834 (2013).
- [4] B. Cao, K. W. Mahmud, and M. Hafezi, *Phys. Rev. A* **94**, 063805 (2016).
- [5] A. Giraldo, B. Krauskopf, N. G. R. Broderick, J. A. Levenson, and A. M. Yacomotti, *New J. Phys.* **22**, 043009 (2020).
- [6] J. Li and D. Cui, *Phys. Rev. A* **107**, 033715 (2023).
- [7] A. A. Gangat, I. P. McCulloch, and G. J. Milburn, *Phys. Rev. X* **3**, 031009 (2013).
- [8] H. Wang, Z. Wang, J. Zhang, Ş. K. Özdemir, L. Yang, and Y. X. Liu, *Phys. Rev. A* **90**, 053814 (2014).
- [9] Y. Jiang, S. Maayani, T. Carmon, F. Nori, and H. Jing, *Phys. Rev. Appl.* **10**, 064037 (2018).
- [10] M. Tavis and F. W. Cummings, *Phys. Rev.* **170**, 379 (1968).
- [11] G. S. Agarwal, *Quantum Optics* (Cambridge University Press, Cambridge, UK, 2013).
- [12] J. Katriel, A. I. Solomon, G. D'Ariano, and M. Rasetti, *Phys. Rev. D* **34**, 2332 (1986).
- [13] C. Emary and T. Brandes, *Phys. Rev. E* **67**, 066203 (2003).
- [14] F. Dimer, B. Estienne, A. S. Parkins, and H. J. Carmichael, *Phys. Rev. A* **75**, 013804 (2007).
- [15] K. Baumann, C. Guerlin, F. Brennecke, and T. Esslinger, *Nature (London)* **464**, 1301 (2010).
- [16] D. Nagy, G. Kónya, G. Szirmai, and P. Domokos, *Phys. Rev. Lett.* **104**, 130401 (2010).
- [17] W. Liu and L. Duan, *Entropy* **25**, 1492 (2023).
- [18] P. Das, D. S. Bhakuni, and A. Sharma, *Phys. Rev. A* **107**, 043706 (2023).
- [19] F. Lingua, G. Mazzarella, and V. Penna, *J. Phys. B* **49**, 205005 (2016).
- [20] A. Richaud and V. Penna, *Phys. Rev. A* **96**, 013620 (2017).
- [21] M. Salado-Mejía, R. Román-Ancheyta, F. Soto-Eguibar, and H. M. Moya-Cessa, *Quantum Sci. Technol.* **6**, 025010 (2021).
- [22] L. Mandel and E. Wolf, *Optical Coherence and Quantum Optics* (Cambridge University Press, Cambridge, UK, 1995).
- [23] M. Hillery and M. S. Zubairy, *Phys. Rev. A* **29**, 1275 (1984).
- [24] D. Aghamalyan, L. Amico, and L. C. Kwek, *Phys. Rev. A* **88**, 063627 (2013).
- [25] L. Amico, D. Aghamalyan, F. Auksztol, H. Crepaz, R. Dumke, and L. C. Kwek, *Sci. Rep.* **4**, 4298 (2014).
- [26] A. I. Solomon, *J. Math. Phys.* **12**, 390 (1971).
- [27] M. Rasetti, *Int. J. Theor. Phys.* **13**, 425 (1975).
- [28] V. Penna and A. Richaud, *Phys. Rev. A* **96**, 053631 (2017).
- [29] A. A. Kirillov, *Elements of the Theory of Representations* (Springer, Berlin, 1976).
- [30] V. Penna, *Phys. Rev. E* **87**, 052909 (2013).
- [31] F. A. Raffa, M. Rasetti, and V. Penna, *Phys. Lett. A* **438**, 128106 (2022).
- [32] L. Hernández-Sánchez, I. Ramos-Prieto, F. Soto-Eguibar, and H. M. Moya-Cessa, *Opt. Lett.* **48**, 5435 (2023).
- [33] S. Sundaram, C. P. Burgess, and D. H. J. O'Dell, *New J. Phys.* **26**, 053023 (2024).
- [34] C. Yuce, A. Kilic, and A. Coruh, *Phys. Scr.* **74**, 114 (2006).
- [35] V. Subramanyan, S. S. Hegde, S. Vishveshwara, and B. Bradlyn, *Ann. Phys.* **435**, 168470 (2021).
- [36] R. Zerimeche, R. Moufok, N. Amouche, and M. Maamache, *Rev. Mex. Fis.* **69**, 010402 (2023).
- [37] G. Lindblad and B. Nagel, *Ann. Inst. Henri Poincaré* **13**, 27 (1970).
- [38] V. Penna, F. A. Raffa, and R. Franzosi, *J. Phys. A: Math. Theor.* **51**, 045301 (2018).
- [39] W.-M. Zhang, D. H. Feng, and R. Gilmore, *Rev. Mod. Phys.* **62**, 867 (1990).
- [40] I. Bloch, J. Dalibard, and W. Zwerger, *Rev. Mod. Phys.* **80**, 885 (2008).